Inorganic Chemistry

pubs.acs.org/IC Communication

Lucky Number 13: A 13-Layer Polytype of the Alkyne Hydrogenation Catalyst CaGaGe

Kelsey L. Hodge, Matthew B. Gray, Wolfgang Windl, and Joshua E. Goldberger*



Cite This: Inorg. Chem. 2021, 60, 14530-14534



ACCESS

Metrics & More



SI Supporting Information

ABSTRACT: Polytypism, the ability of materials to form crystal structures with different stacking sequences, occasionally causes materials with the same stoichiometry and similar local structures to have profoundly different properties. Herein, we discover a metastable 13-layer trigonal (13T) polytype of CaGaGe, a layered intermetallic phase comprised of [GaGe]²⁻ honeycombs separated by Ca²⁺. 13T-CaGaGe is synthesized from arc-melting the elements, and its structure is elucidated via neutron powder diffraction. Air-stable 13T-CaGaGe has one misaligned [GaGe]²⁻ layer for every 13 and transforms into the more stable 4-layer hexagonal (4H) CaGaGe polytype after annealing at 500 °C. Transition-metal-free 13T-CaGaGe shows remarkable activity in the catalytic hydrogenation of phenylacetylene to styrene and ethylbenzene, much higher than the 4H polytype. This work identifies the first 13-layer polytype for any crystal structure and further establishes the influence of polytypism on catalysis.

olymorphs, compounds with the same stoichiometry and different crystal structures, are prevalent in materials chemistry. Polytypism is a subset of polymorphism commonly occurring in layered compounds describing materials having nearly identical structures and compositions along two dimensions but stacked into unit cells with different repeating sequences. While most polytypes lead to subtle differences in structure and properties, sometimes dramatic changes are observed. Namely, TaSe_{2-x}Te_x exhibits an order of magnitude higher superconducting transition temperature in the 3-layer rhombohedral polytype compared to the 2-layer hexagonal polytype, despite minimal differences in their local coordination. SiC forms many different polytypes of close-packed corner-sharing tetrahedra, and its band gap changes from 2.39 eV (zinc blende) to 3.33 eV (wurtzite). Finally, there have been significant differences in the catalytic and electrocatalytic behavior between the face-centered-cubic and the 4-layer hexagonal (4H) polytypes of Au and Cu, which have different arrangements of close-packed layers.3-6 4H-Cu has been recently found to exhibit higher electrocatalytic activities and ethylene selectivity in the CO₂ reduction reaction.⁴ Thus, polytypism can significantly influence the catalytic behavior.

An exciting family of materials that feature polytypism are Zintl–Klemm compounds, having structures comprised of layers of main-group elements separated by large electropositive cations. ^{1,7–14} These materials exhibit many exotic physical properties including axis-dependent conduction polarity in NaSn₂As₂, ¹⁵ hydrogen absorption in SrGa₂, ¹⁶ and topological insulating properties of BaSn₂. ^{11,17} Examples of polytypism in these phases include CaGe₂, forming 2- and 6-layer polytypes, and CaAlSi, forming 1-, 5-, and 6-layer polytypes.

Recently, we discovered that the transition-metal-free layered Zintl-Klemm compound BaGa₂ shows catalytic activities for the hydrogenation of phenylacetylene into styrene and ethylbenzene within an order of magnitude of Pd-based

compounds.²⁰ BaGa₂ consists of planar layers of covalently bonded Ga- honeycombs, where every Ga formally has 7 valence electrons, ignoring weak intralayer Ga-Ga π bonding. We hypothesized that the valence electron count of 7 makes these phases acidic, promoting adsorption of both H2 and alkynes. We found other structurally and electronically similar Zintl phases to have appreciable catalytic activity for alkyne hydrogenation.²¹ One such material is CaGaGe, which is comprised of puckered honeycomb [GaGe]²⁻ layers having an alternating BN-like arrangement, with each layer separated by Ca²⁺.²² According to the Zintl-Klemm electron-counting rules, each Ga- and Ge- formally has 7 and 8 valence electrons, respectively. CaGaGe adopts a 4H-YPtAs structure type, in which the Ga atoms in neighboring layers tilt toward each other, partially stabilizing the lack of an octet. The interlayer Ga-Ga distance is too large (3.57 Å) to form a covalent bond (Figure 1a).²² Because each Ge formally has an octet, the layers tilt to minimize the electrostatic repulsion between the Ge atoms and the nearest Ge or Ga atoms in neighboring layers. Transmission electron microscopy studies suggested that CaGaGe could form a more complex stacking sequence, although the structure was never determined. Herein, we have elucidated a new 13-layer trigonal (13T) polytype of CaGaGe, an air-stable, highly active heterogeneous catalyst for the hydrogenation of alkynes with consistently greater activities than those of the 4H polytype.

CaGaGe was synthesized by arc-melting stoichiometric amounts of the elements. The initial Rietveld refinements

Received: July 6, 2021 Published: September 17, 2021





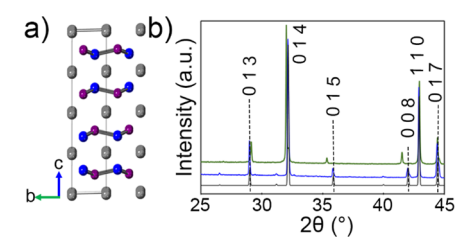


Figure 1. (a) 4H polytype of CaGaGe. (b) XRD patterns of synthesized 13T (green), synthesized 4H (blue), and calculated 4H-CaGaGe (black), with Miller indices labeling the 4H polytype.

were performed using X-ray diffraction (XRD). All attempts to fit the pattern to the 4H $P6_3/mmc$ crystal structure were unsuccessful (Figures 1a,b and S1-S3). When assuming a 4H polytype, all 0kl reflections, where l is odd are shifted to either higher or lower 2θ , and additional unindexed weak reflections are present (Figure S2). However, the observed intensity of every reflection is close to that predicted for the 4H polytype, indicating that the majority phase has a similar structure but a different stacking sequence. Indeed, the d spacings of the 0kl reflections and the new minor reflections precisely match a 13-layer unit cell (Figure 2a and S3). The 4H-CaGaGe phase is

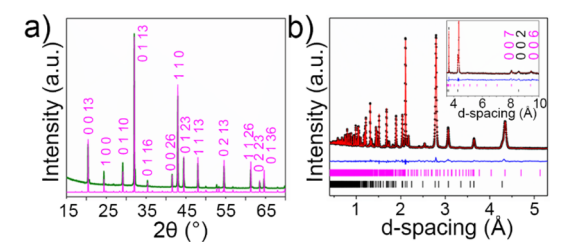


Figure 2. (a) Observed (green) and superimposed calculated (magenta) XRD patterns of P3 CaGaGe. (b) Rietveld refinement of the NPD. The observed data, calculated pattern, and difference curve are represented by black dots, red lines, and blue lines, respectively. The *hkl* marks for the 13T and 4H phases are magenta and black, respectively. The inset shows another frame highlighting the 006 and 007 reflections of 13T-CaGaGe and the 002 reflection of 4H-CaGaGe.

present as a minor phase (\sim 15 wt %), appearing as shoulders on the most intense 13-layer reflections, at slightly larger 2θ . The 13-layer phase transforms into the 4H polytype upon annealing at 500 °C for 18 h (Figure 1b). No well-defined transition is observed with differential scanning calorimetry, suggesting that the polytypes have similar energies (Figure S4).

Time-of-flight neutron powder diffraction (NPD) was performed to elucidate the structure of this 13-layer phase because the neutron scattering factors of Ga and Ge are considerably different (Ga = 6.83; Ge = 8.6). Rietveld refinement convincingly established a 13-layer unit cell as the majority phase (Figure 2b). The most visually straightforward evidence of the 13-layer structure is the presence of the 006 and 007 reflections at large d spacings (Figure 2b, inset). Between those reflections, the 002 reflection of the minority 4H phase is apparent.

A combination of Rietveld refinements and density functional theory (DFT) calculations indicated that this new polytype crystallizes into a P3 space group, as described in Figures S5–S11 and Tables S1 and S2. The refined 13T-CaGaGe P3 crystal structure (Figure 3) is nearly identical with the crystal structure of 4H-CaGaGe, except for "layer 8".

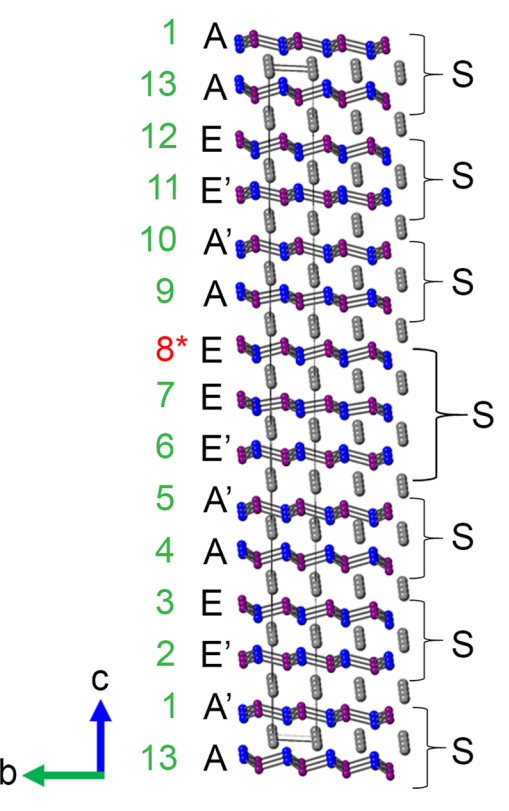


Figure 3. Refined *P*3 crystal structure of CaGaGe. Ca, Ga, and Ge are represented with gray, blue, and purple spheres, respectively. The green text refers to the GaGe layer number. The unique 8th layer is highlighted in red. "A" and "E" in the left column indicate whether "Ga" or "Ge", respectively, occupy the left $(^1/_3, ^2/_3, z)$ positions. An apostrophe next to A or E denotes that the right $(^2/_3, ^1/_3, z)$ atom is above the left $(^1/_3, ^2/_3, z)$ atom. The "S" label groups layers having the same atoms stacked on top of each other.

Except for this layer, the positions of the Ga and Ge atoms alternate every two layers. The Ga atoms pucker toward each other to partially stabilize the lack of an octet, but the average Ga—Ga interlayer distance [3.45(14) Å] is too large for full covalent bonding. Layer 8 deviates from the 4H-stacking sequence and lacks interlayer Ga—Ga stabilization. In summary, 13T-CaGaGe has an overall repeat unit of 3 \times 4H-CaGaGe capped by one deviating CaGaGe layer.

Considering the similarity of the 13T and 4H phases, one could envision other polytypes. DFT calculations of the formation energies of the 4H, 4n + 1, and 4n - 1 polytypes (n = 1-4) confirmed that the 4H polytype was the most stable structure (Table S3). The energetic penalty of adding or subtracting an additional layer was calculated as a stacking fault energy relative to the 4H polytype and normalized per formula unit of CaGaGe. The stacking fault energies in the 5, 9, 13, and 17 (4n + 1) polytypes (67-73 meV) were much smaller than those in the 3, 7, 11, and 15 (4n - 1) polytypes (129-139)meV). The extra energetic penalty in the 4n-1 polytypes results from the destabilizing influence of having Ge and Ga atoms in the neighboring layers tilted toward each other (Figure S12). This destabilizing interlayer Ge/Ga interaction is absent in the 4n + 1 polytypes. Although the other 4n + 1polytypes are all close in formation energy, no evidence for these structures was observed in the XRD or NPD patterns. Nevertheless, this 13T phase is metastable and can only be accessed from the fast cooling achieved via arc-melting. To the

best of our knowledge, this is the first example of a crystal structure with a 13-layer polytype in any crystalline material, including materials known to have many polytypes (zeolites, SiC, etc.). The only previous claim of a 13-layer polytype was $Ba_{18}Ti_{54}Nb_2O_{132}$, although its atomic structure remains undetermined. ²⁴

The catalytic activities of the 13T and 4H phases in the hydrogenation of phenylacetylene to styrene and ethylbenzene were evaluated in dimethylformamide (DMF) and n-butanol (n-BuOH) at 51 bar of H₂ (Figure 4a), a common pressure for

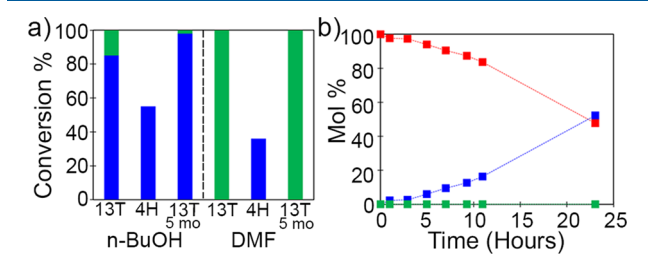


Figure 4. (a) Catalytic hydrogenation of phenylacetylene to styrene (blue) or ethylbenzene (green) using either non-air-exposed 13T- or 4H-CaGaGe and 5 month air-exposed 13T-CaGaGe as catalysts. Reaction conditions are 51 bar of H₂, 20 h, 2.5 mL of solvent (*n*-BuOH or DMF), 1.82 mmol of phenylacetylene, and 0.12 mmol of CaGaGe (6.2 mol %). (b) Time-dependent conversion of phenylacetylene (red) to styrene (blue) using non-air-exposed 13T-CaGaGe at 1 bar of H₂, in 2.5 mL of DMF, 0.91 mmol of phenylacetylene, and 0.081 mmol of CaGaGe (8.2 mol %). Ethylbenzene (green) was not detected.

catalyst screening. 25-27 After 24 h, 13T-CaGaGe completely hydrogenates phenylacetylene to ethylbenzene in DMF and is more selective for semihydrogenation to styrene in n-BuOH. Surprisingly, 13T-CaGaGe shows much greater conversion than the 4H-CaGaGe phase, despite a nearly identical structure and an average particle size. This observation is quite robust, and the enhanced activity in 13T-CaGaGe was maintained across three synthetic batches of both polytypes. Additionally, 13T-CaGaGe has enhanced air stability compared to other Zintl-Klemm catalysts, including BaGa₂, which loses all activity upon immediate exposure to air. ^{20,21} After 5 months in air, 13T-CaGaGe retained complete conversion with similar product mixtures in DMF and n-BuOH, using these same reaction conditions. No new phases are observed in the diffraction pattern, further evidencing its air stability (Figure S13). Additionally, cyclability experiments in n-BuOH demonstrated a minimal loss in activity after 5 cycles (Figure

13T-CaGaGe even exhibited catalytic activity at 1 bar of H_2 (Figure 4b). The time-dependent conversion in DMF shows >50% conversion after 23 h. The surface specific activity (SSA) was estimated by measuring the surface area per gram of catalyst (0.406 m² g⁻¹) with the Kr adsorption isotherm Braunauer–Emmett–Teller (BET) method along with conversion versus time (Figure S15). Using the 23 h conversion, the SSA is estimated to be 315 h⁻¹, similar to those of Lindlar's catalyst (650 h⁻¹) and other highly active Pd- and Aucontaining catalysts (Table S4). 20,21,28 An induction period is apparent, which complicates further kinetic analysis, and makes the estimate of SSA a lower bound. Inductively coupled plasma optical emission spectrometry analysis of the supernatant indicated that the amounts of soluble Ga and Ge were <1 ppm,

suggesting that catalysis is not due to a soluble Ga- or Gebased impurity.

The difference in activity between these polytypes is unexpected. Because the 4H-CaGaGe phase is prepared by annealing the 13T phase at 500 °C in fused silica, we explored whether the reduced activity in 4H-CaGaGe was caused by greater degrees of surface oxidation upon annealing. However, the X-ray photoelectron spectroscopy (XPS) spectra of the 13T and 4H powders show no differences in the degree of oxidation between the polytypes (Figure S16). Both phases show major Ga $2p_{3/2}$ and $2p_{1/2}$ peaks at 1117.90 and 1144.5 eV, indicative of an oxidized Ga³⁺, along with shoulders at 1115.7 and 1142.7 eV, which are at lower energies than Ga⁰ and thus indicative of an anionic Ga surface species.²⁹ The presence of this anionic Ga surface species was shown to correlate with the catalytic activity in ${\rm \tilde{B}aGa_2.}^{20}$ The relative areas of the anionic Ga shoulders are nearly identical in both 4H-CaGaGe and 13T-CaGaGe, indicating that the degree of surface oxidation is very similar. The Ge 2p and O 1s regions in the XPS spectra of the two polytypes are also similar (Figure S17). Thus, the difference in activity between the polytypes does not result from varying degrees of surface oxidation. The higher activity in the 13T phase could originate from a much more active misfit layer. Another possibility is that the subtle differences in the Ga-Ge bond length lead to enhanced activity. The 13T polytype has, on average, a slightly smaller Ga-Ge bond distance of 2.507(23) Å, ranging from 2.458 to 2.541 Å compared to 4H-CaGaGe [2.530(3) Å]. In other heterogeneous catalysts, similar metal-metal bond length deviations significantly influence the catalytic activity. One final possibility is that the surface structure of the arc-melted 13T phase exists in a nonequilibrium state, with a higher concentration of catalytically active defects and amorphous regions. The concentration of these regions is decreased upon annealing to form the 4H phase. Further investigations are needed to conclusively pinpoint the exact nature of the active sites and origin of increased activity in the 13T polytype.

This exotic, metastable 13T-CaGaGe is the first 13-layer polytype and provides an additional example of the unique role of polytypism on the catalytic performance, beyond Cu and Au. Its formation is highly reproducible, and it is the dominant phase that forms through >50 syntheses. This highly active transition-metal-free, air-stable catalyst paves the way for exploration of the reactivity, substrate selectivity and functional group tolerance, robustness, and mechanistic understanding of catalysis with these Zintl–Klemm polytypes.

ASSOCIATED CONTENT

Supporting Information

The Supporting Information is available free of charge at https://pubs.acs.org/doi/10.1021/acs.inorgchem.1c02051.

Experimental methods, general procedure for refinements, tables of refinement results, XPS, BET, recycling experiments, and air-stability studies (PDF)

Accession Codes

CCDC 2096945 contains the supplementary crystallographic data for this paper. These data can be obtained free of charge via www.ccdc.cam.ac.uk/data_request/cif, or by emailing data_request@ccdc.cam.ac.uk, or by contacting The Cambridge Crystallographic Data Centre, 12 Union Road, Cambridge CB2 1EZ, UK; fax: +44 1223 336033.

AUTHOR INFORMATION

Corresponding Author

Joshua E. Goldberger – Department of Chemistry and Biochemistry, The Ohio State University, Columbus, Ohio 43210, United States; orcid.org/0000-0003-4284-604X; Email: Goldberger.4@osu.edu

Authors

Kelsey L. Hodge — Department of Chemistry and Biochemistry, The Ohio State University, Columbus, Ohio 43210, United States

Matthew B. Gray – Department of Chemistry and Biochemistry, The Ohio State University, Columbus, Ohio 43210, United States; orcid.org/0000-0002-9526-4732

Wolfgang Windl — Department of Materials Science and Engineering, The Ohio State University, Columbus, Ohio 43210, United States

Complete contact information is available at: https://pubs.acs.org/10.1021/acs.inorgchem.1c02051

Author Contributions

The manuscript was written through contributions of all authors.

Notes

The authors declare no competing financial interest.

ACKNOWLEDGMENTS

K.L.H. and J.E.G. gratefully acknowledge Caitlin Bien and Casey Wade for BET measurements. This work was primarily supported by the Center of Emergent Materials an NSF MRSEC, under Award DMR-2011876. XPS work was supported by NSF-DMR Grant 0114098. A portion of this research used resources at Spallation Neutron Source, a Department of Energy, Office of Science User Facility, operated by the Oak Ridge National Laboratory. W.W.'s contributions were funded by the AFOSR, Award FA9550-21-1-0268, program director Dr. Ali Sayir. W.W. thanks the Ohio Supercomputer Center for supercomputing resources under project number PA0072.

REFERENCES

- (1) Luo, H. X.; Xie, W. W.; Tao, J.; Inoue, H.; Gyenis, A.; Krizan, J. W.; Yazdani, A.; Zhu, Y. M.; Cava, R. J. Polytypism, polymorphism, and superconductivity in TaSe_{2-x}Te_x. *Proc. Natl. Acad. Sci. U. S. A.* **2015**, *112*, E1174–E1180.
- (2) Park, C. H.; Cheong, B. H.; Lee, K. H.; Chang, K. J. Structural and Electronic Properties of Cubic, 2H, 4H, and 6H SiC. *Phys. Rev. B: Condens. Matter Mater. Phys.* **1994**, 49, 4485–4493.
- (3) Chen, Y.; Fan, Z. X.; Luo, Z. M.; Liu, X. Z.; Lai, Z. C.; Li, B.; Zong, Y.; Gu, L.; Zhang, H. High-Yield Synthesis of Crystal-Phase-Heterostructured 4H/fcc Au@Pd Core-Shell Nanorods for Electrocatalytic Ethanol Oxidation. *Adv. Mater.* 2017, 29, 1701331.
- (4) Chen, Y.; Fan, Z. X.; Wang, J.; Ling, C. Y.; Niu, W. X.; Huang, Z. Q.; Liu, G. G.; Chen, B.; Lai, Z. C.; Liu, X. Z.; Li, B.; Zong, Y.; Gu, L.; Wang, J. L.; Wang, X.; Zhang, H. Ethylene Selectivity in Electrocatalytic CO₂ Reduction on Cu Nanomaterials: A Crystal Phase-Dependent Study. J. Am. Chem. Soc. **2020**, 142, 12760–12766.
- (5) Fan, Z. X.; Luo, Z. M.; Chen, Y.; Wang, J.; Li, B.; Zong, Y.; Zhang, H. Synthesis of 4H/fcc-Au@M (M = Ir, Os, IrOs) Core-Shell Nanoribbons For Electrocatalytic Oxygen Evolution Reaction. *Small* **2016**, *12*, 3908–3913.
- (6) Han, S. B.; Xia, G. J.; Cai, C.; Wang, Q.; Wang, Y. G.; Gu, M.; Li, J. Gas-Assisted Transformation of Gold From fcc to the Metastable 4H Phase. *Nat. Commun.* **2020**, *11*, 552.

- (7) Bojin, M. D.; Hoffmann, R. The REME Phases I. An Overview of Their Structural Variety. *Helv. Chim. Acta* **2003**, *86*, 1653–1682.
- (8) Bojin, M. D.; Hoffmann, R. The REME Phases II. What's Possible? Helv. Chim. Acta 2003, 86, 1683-1708.
- (9) Brown, S. R.; Kauzlarich, S. M.; Gascoin, F.; Snyder, G. J. Yb₁₄MnSb₁₁: New High Efficiency Thermoelectric Material for Power Generation. *Chem. Mater.* **2006**, *18*, 1873–1877.
- (10) Evans, M. J.; Wu, Y.; Kranak, V. F.; Newman, N.; Reller, A.; Garcia-Garcia, F. J.; Haussermann, U. Structural Properties and Superconductivity in the Ternary Intermetallic Compounds MAB (M = Ca, Sr, Ba; A = Al, Ga, In; B = Si, Ge, Sn). *Phys. Rev. B: Condens. Matter Mater. Phys.* **2009**, *80*, 064514.
- (11) Kim, S. J.; Fassler, T. F. Crystal Structure of Barium Distannide, BaSn₂. Z. Kristallogr. New Cryst. Struct. **2008**, 223, 325–326.
- (12) Kim, S. J.; Hu, S. Q.; Uher, C.; Kanatzidis, M. G. Ba₄In₈Sb₁₆: Thermoelectric Properties of a New Layered Zintl Phase With Infinite Zigzag Sb Chains and Pentagonal Tubes. *Chem. Mater.* **1999**, *11*, 3154–3159.
- (13) Owens-Baird, B.; Wang, J.; Wang, S. G.; Chen, Y. S.; Lee, S.; Donadio, D.; Kovnir, K. III-V Clathrate Semiconductors with Outstanding Hole Mobility: $Cs_8In_{27}Sb_{19}$ and $A_8Ga_{27}Sb_{19}$ (A = Cs, Rb). *J. Am. Chem. Soc.* **2020**, *142*, 2031–2041.
- (14) Owens-Baird, B.; Xu, J. Y.; Petrovykh, D. Y.; Bondarchuk, O.; Ziouani, Y.; Gonzalez-Ballesteros, N.; Yox, P.; Sapountzi, F. M.; Niemantsverdriet, H.; Kolen'ko, Y. V.; Kovnir, K. NiP₂: A Story of Two Divergent Polymorphic Multifunctional Materials. *Chem. Mater.* **2019**, *31*, 3407–3418.
- (15) He, B.; Wang, Y. X.; Arguilla, M. Q.; Cultrara, N. D.; Scudder, M. R.; Goldberger, J. E.; Windl, W.; Heremans, J. P. The Fermi Surface Geometrical Origin of Axis-Dependent Conduction Polarity in Layered Materials. *Nat. Mater.* **2019**, *18*, 568–572.
- (16) Wenderoth, P.; Kohlmann, H. In Situ Neutron Powder Diffraction of the Formation of SrGa₂D₂, and Hydrogenation Behavior of YbGa₂ and EuGa₂. *Inorg. Chem.* **2013**, *52*, 10525–10531.
- (17) Trout, A. H.; Hodge, K. L.; Scudder, M.; Goldberger, J. E.; McComb, D. W. Low-Pressure Induced Disproportionation of Barium Distannide. *J. Phys. Chem. C* **2021**, *125*, 15496–15502.
- (18) Cultrara, N. D.; Wang, Y. X.; Arguilla, M. Q.; Scudder, M. R.; Jiang, S. S.; Windl, W.; Bobev, S.; Goldberger, J. E. Synthesis of 1T, 2H, and 6R Germanane Polytypes. *Chem. Mater.* **2018**, 30, 1335–1343.
- (19) Sagayama, H.; Wakabayashi, Y.; Sawa, H.; Kamiyama, T.; Hoshikawa, A.; Harjo, S.; Uozato, K.; Ghosh, A. K.; Tokunaga, M.; Tamegai, T. Two Types of Multistack Structures in MgB₂-Type Superconductor CaAlSi. *J. Phys. Soc. Jpn.* **2006**, *75*, 043713.
- (20) Hodge, K. L.; Goldberger, J. E. Transition Metal-Free Alkyne Hydrogenation Catalysis with BaGa₂, a Hydrogen Absorbing Layered Zintl Phase. *J. Am. Chem. Soc.* **2019**, *141*, 19969–19972.
- (21) Hodge, K. L.; Goldberger, J. E., Alkyne Hydrogenation Catalysis across a Family of Ga/In Layered Zintl Phases. ACS Appl. Mater. Interfaces 2021. DOI: 10.1021/acsami.1c10358
- (22) Czybulka, A.; Pinger, B.; Schuster, H.-U. Neue Erdalkali-Gallium-Silicide, -Germanide und -Stannide Mit Vom AIB2-Typ Abgeleiteten Strukturen. Z. Anorg. Allg. Chem. 1989, 579, 151–157.
- (23) Sears, V. F. Neutron Scattering Lengths and Cross Sections. *Neutron News* **1992**, *3*, 26–37.
- (24) Roth, R. S.; Ettlinger, L. D.; Parker, H. S. Phase Equilibria and Crystal Chemistry in the Ternary System BaO-TiO₂-Nb₂O₅. *J. Solid State Chem.* **1987**, *68*, 330–339.
- (25) Chieffi, G.; Giordano, C.; Antonietti, M.; Esposito, D. FeNi Nanoparticles with Carbon Armor as Sustainable Hydrogenation Catalysts: Towards Biorefineries. *J. Mater. Chem. A* **2014**, *2*, 11591.
- (26) Ye, T. N.; Lu, Y. F.; Li, J.; Nakao, T.; Yang, H. S.; Tada, T.; Kitano, M.; Hosono, H. Copper-Based Intermetallic Electride Catalyst for Chemoselective Hydrogenation Reactions. *J. Am. Chem. Soc.* 2017, 139, 17089–17097.
- (27) Hardacre, C.; Mullan, E. A.; Rooney, D. W.; Thompson, J. M.; Yablonsky, G. S. Comparison of mass transfer effects in the

heterogeneously catalysed hydrogenation of phenyl acetylene in heptane and an ionic liquid. *Chem. Eng. Sci.* **2006**, *61*, 6995–7006.

- (28) Kuwahara, Y.; Kango, H.; Yamashita, H. Pd Nanoparticles and Aminopolymers Confined in Hollow Silica Spheres as Efficient and Reusable Heterogeneous Catalysts for Semihydrogenation of Alkynes. *ACS Catal.* **2019**, *9*, 1993–2006.
- (29) Schön, G. Auger and direct electron spectra in X-ray photoelectron studies of zinc, zinc oxide, gallium and gallium oxide. *J. Electron Spectrosc. Relat. Phenom.* **1973**, *2*, 75–86.
- (30) Wexler, R. B.; Martirez, J. M. P.; Rappe, A. M. Chemical Pressure-Driven Enhancement of the Hydrogen Evolving Activity of Ni₂P from Nonmetal Surface Doping Interpreted via Machine Learning. J. Am. Chem. Soc. 2018, 140, 4678–4683.